Q. J. R. Meteorol. Soc. (2006), **132**, pp. 1627–1643 doi: 10.1256/qj.05.139

Subscale forcing in a global atmospheric circulation model and stochastic parametrization

By RITA SEIFFERT, RICHARD BLENDER and KLAUS FRAEDRICH*
Meteorologisches Institut, Universität Hamburg, Germany

(Received 1 July 2005; revised 7 November 2005)

SUMMARY

A global atmospheric circulation model is used to derive the properties of the subscale forcing in the primitive equations. The study is based on a simulation with the model PUMA (Portable University Model of the Atmosphere), which represents a dynamical core with linear diabatic heating and friction. The subscale forcing is determined for a low wave number resolution $T21$ ($\approx 5° \times 5°$) embedded in $T42$ resolution ($\approx 2.5° \times 2.5°$) using the differences between the low wave number filtered $T42$ model and the forcing by low wave numbers ($T21$). The mean subscale forcing vanishes (besides a small heating contribution). The variance has largest values in the midlatitudes for vorticity (mid-troposphere), temperature (lower troposphere), and in the polar mid-troposphere for divergence. The temporal correlations reveal a slow decay in the first few hours followed by an exponential decay with an e-folding time of about one day. The correlation with hyperdiffusion ($\sim\nabla^8$) is below 0.4. Based on these results the design of stochastic parametrizations is suggested.

KEYWORDS: Eddy viscosity Primitive equations Subgrid variability

1. INTRODUCTION

Finite resolutions in atmospheric circulation models constrain the complete nonlinear interactions, which requires provisions to yield a simulation of the realistic equilibrium state determined by the interaction of all scales. In particular, the cascades of energy and enstrophy predicted by two-dimensional (2D) turbulence theory are disturbed. The neglect of small scales alters the large-scale behaviour, and hence the simulated climate mean and the variability. The traditional theory of 2D turbulence (Kraichnan 1976) predicts two inertial subranges: for large scales the indirect energy cascade reveals an energy spectrum proportional to $k^{-5/3}$, and for small scales a direct enstrophy cascade with k^{-3}. Both subranges are separated by the forcing range. However, this theory demands infinite domains and leads to problems with the energy sink for vanishing total wave number in numerical models. The atmosphere is characterized by a broad forcing range, mainly determined by baroclinic instability, associated with an approximate enstrophy range, but no energy cascading range (Boer and Shepherd 1983). In the range of the lowest wave numbers, backscatter towards higher wave numbers occurs, which acts as an additional source and leads to a further direct enstrophy cascade. Considering wave and rotational modes separately, Bartello *et al.* (1996) find that wave modes are damped, whereas rotational modes are forced by subscale modes (by a negative eddy viscosity). The large-scale energy spectrum depends crucially on the choice of the dissipation (Ekman damping or hyperdiffusion) and on the type of forcing (Tran and Shepherd 2002). Thus the structure of the atmospheric energy spectrum and the existence of the two cascades remains an open problem.

The downscale interactions are parametrized by eddy viscosity or hyperdiffusion ($\sim\nabla^{2h}$). These parametrizations are also beneficial for the numerical stability of the codes. Koshyk and Boer (1995) and Kaas *et al.* (1999) relate the subscale forcing to the spectral horizontal diffusion in observations and general circulation model (GCM) simulations. The upscale interaction can be incorporated as stochastic forcing, which accounts for the irregular and unpredictable nature of the subgrid processes.

* Corresponding author: Meteorologisches Institut, Universität Hamburg, Bundesstrasse 55, D-20146 Hamburg, Germany. e-mail: klaus.fraedrich@zmaw.de

A part of the upscale interaction can be considered as a backscatter effect and parametrized by deterministic negative hyperdiffusion (Frederiksen and Davis 1997).

A justification of the stochastic forcing within dynamical systems theory is given by Palmer (2001). Stochastic parametrizations are included in the ECMWF model (Buizza *et al.* 1999, 2000; Shutts 2001) and improve the precipitation simulation (see Theis *et al.* 2003). In mesoscale convective systems this problem has been considered by Lin and Neelin (2000, 2002). The effect of unresolved variability has been parametrized by the inclusion of noise, and interpreted as additional damping in terms of a fluctuation–dissipation relation (von Storch 2004). The impact of stochastic forcing in general circulation models has been analysed in ensemble simulations by Pérez-Muñuzuri *et al.* (2003, 2005). They show that stochastic forcing can lead to enhanced order and coherence, whereas the traditional point of view emphasizes the excitation of instabilities and disorder. The stochastic parametrizations in these models are based on simple assumptions for the statistical properties, and the forcing is either uncorrelated in space and time or with constant magnitudes within finite regions and time intervals. So far, there is no systematic treatment of this problem in GCMs except for a project at the European Centre for Medium-Range Weather Forecasts (ECMWF), which addresses the unknown stochastic forcing (Hoskins *et al.* 2004). There, a very high resolution version of the forecast model ($T799$) is compared with a lower resolution version ($T95$) to derive the subscale processes.

Our aim is to analyse the dynamic subscale processes in a GCM simulation to derive quantitative properties of stochastic parametrizations for low resolution GCMs in long-term climate simulations. The atmospheric circulation model PUMA (Portable University Model of the Atmosphere), which is driven by simple diabatic forcings, is a GCM restricted to the dynamical core of the primitive equations. It presents a well-defined physical setting since it avoids problems due to model-specific diabatic parametrizations. The simulation is performed in a moderately high resolution ($T42$, $\approx 2.5^\circ \times 2.5^\circ$) environment where all scales are included explicitly and the subscale forcing is extracted numerically after the definition of an intermediate cut-off scale ($T21, \approx 5^\circ \times 5^\circ$). The approach is described by Domaradzki *et al.* (1987) for the Navier–Stokes equations. It was applied later to passive scalar turbulence (Lesieur and Rogallo 1989) and to an assessment of the different properties of rotational and wave modes (Bartello *et al.* 1996). The properties of these residual terms are subjected to statistical analyses in grid and wave number space to detect the main physical properties.

In section 2 the dynamical model is described and in section 3 the experimental design for the analysis of the subscale forcing is specified. In section 4 the results for the statistical analysis of the subscale forcing are presented. A summary and an outlook on the application to stochastic parametrization conclude in section 5.

2. Model

PUMA (Fraedrich *et al.* 2005a) is an atmospheric global circulation model based on the multi-layer primitive equations (see Hoskins and Simmons 1975; James and Gray 1986); the prognostic equations for vorticity ζ and horizontal divergence D, the hydrostatic approximation, the continuity equation and the thermodynamic equation are

$$\frac{\partial(\zeta + f)}{\partial t} = \frac{1}{(1-\mu^2)}\frac{\partial \mathcal{F}_v}{\partial \lambda} - \frac{\partial \mathcal{F}_u}{\partial \mu} - \frac{\zeta}{\tau_F} + H_\zeta, \tag{1}$$

$$\frac{\partial D}{\partial t} = \frac{1}{(1-\mu^2)}\frac{\partial \mathcal{F}_u}{\partial \lambda} + \frac{\partial \mathcal{F}_v}{\partial \mu} - \nabla^2\left(\frac{U^2+V^2}{2(1-\mu^2)} + \Phi + T_0 \ln p_s\right) - \frac{D}{\tau_F} + H_D, \quad (2)$$

$$\frac{\partial \Phi}{\partial(\ln \sigma)} = -T, \quad (3)$$

$$\frac{\partial(\ln p_s)}{\partial t} = -\frac{U}{1-\mu^2}\frac{\partial(\ln p_s)}{\partial \mu} - D - \frac{\partial \dot{\sigma}}{\partial \sigma}, \quad (4)$$

$$\frac{\partial T'}{\partial t} = -\frac{1}{(1-\mu^2)}\frac{\partial(UT')}{\partial \lambda} - \frac{\partial(VT')}{\partial \mu} + DT' - \dot{\sigma}\frac{\partial T}{\partial \sigma} + \kappa\frac{T}{p}\omega + \frac{T_R - T}{\tau_R} + H_T, \quad (5)$$

with

$$\mathcal{F}_u = V(\zeta + f) - \dot{\sigma}\frac{\partial U}{\partial \sigma} - T'\frac{\partial(\ln p_s)}{\partial \lambda},$$

$$\mathcal{F}_v = -U(\zeta + f) - \dot{\sigma}\frac{\partial V}{\partial \sigma} - T'(1-\mu^2)\frac{\partial(\ln p_s)}{\partial \mu}.$$

The temperature $T = T_0 + T'$ is separated into a constant reference temperature T_0 and an anomaly T'. The horizontal coordinates are $\mu = \sin\varphi$ with the latitude φ and the longitude λ. The vertical coordinate is $\sigma = p/p_s$, where p and p_s denote pressure and surface pressure. U and V are the zonal and meridional wind components multiplied by $\cos\varphi$. The vertical velocity in σ-coordinates is $\dot{\sigma} = \mathrm{d}\sigma/\mathrm{d}t$, $\omega = \mathrm{d}p/\mathrm{d}t$ is the vertical velocity in the p-system, Φ denotes the geopotential, κ is the adiabatic coefficient, and f the Coriolis parameter.

Newtonian cooling, $(T_R - T)/\tau_R$, parametrizes the heating processes relaxing temperature towards a prescribed restoration temperature field T_R with the time-scale τ_R. T_R is zonally symmetric with an equator–pole gradient of 70 K without annual or daily cycle. That is, the subsequent experiments represent an aqua-planet at equinox conditions. The vertical distribution in the troposphere is given by a lapse rate of 0.0065 K m^{-1}. The restoration time-scale τ_R is 30 days in the top three levels, 10 days in the second lowest and 5 days in the lowest level. Due to the absence of an explicit precipitation parametrization, tropical perturbations, which strongly depend on evaporation and precipitation, are under-represented.

Rayleigh friction, which describes surface drag and turbulent exchange of momentum in the boundary layer, damps vorticity and divergence with the time-scale τ_F. Rayleigh friction acts only in the lowest level with the time-scale $\tau_F = 1$ day. H_ζ, H_D and H_T denote the hyperdiffusion in (1), (2) and (5). For a prognostic variable Q, the hyperdiffusion is

$$H_Q = -(-1)^h K \nabla^{2h} Q \quad (6)$$

with $h = 4$ and a diffusion coefficient K which is the same for all variables. Hyperdiffusion provides the energy cascading into subgrid scales and its dissipation. The diffusion coefficient K is chosen to damp the smallest resolved wave in $T42$ with a time-scale of 0.25 days. Horizontal fields are represented by triangular truncated series of spherical harmonics with $T42$ resolution. In the vertical, five equally spaced σ-levels are used. While linear terms are calculated in the spectral domain, nonlinear products are computed in grid-point space.

Before the differences between low and high resolution are examined, the climatologies of the mean circulation and its variability are presented. The zonal mean circulation of PUMA (Fig. 1) shows the midlatitude jet streams (left panels) and the zonal-mean circulation (right panels). The high resolution simulation ($T42$) in the upper

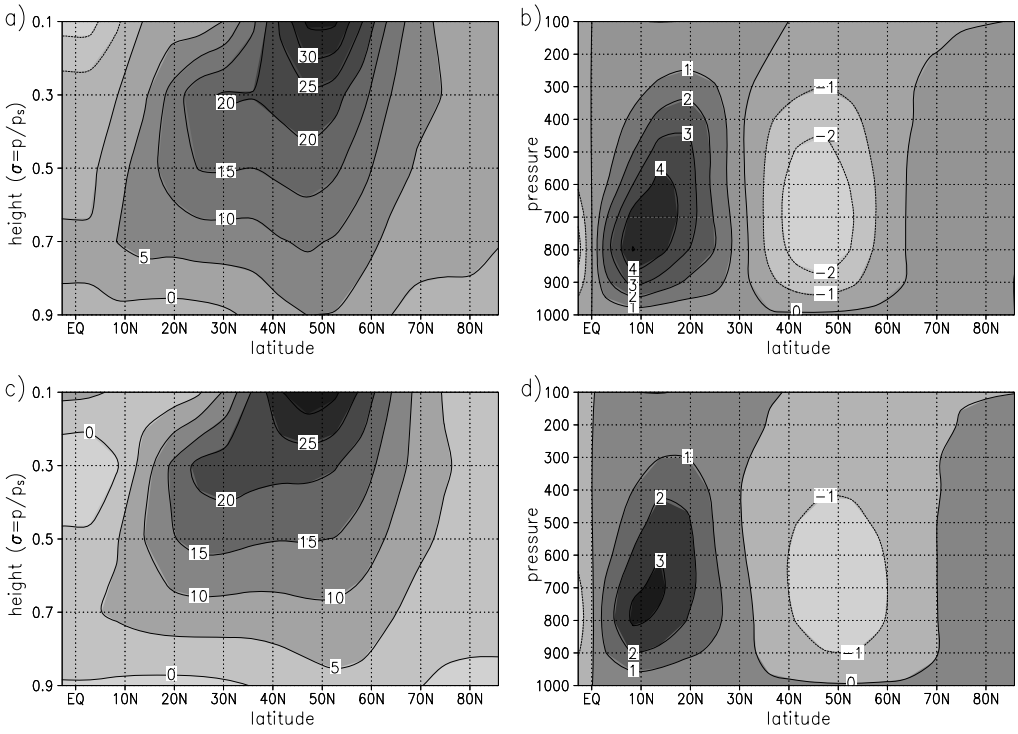

Figure 1. Zonally averaged zonal wind (a), (c) (m s^{-1}) and meridional stream function (b), (d) (10^{10} kg s^{-1}) for simulations with high resolution $T42$ (a), (b) and low resolution $T21$ (c), (d).

panels reveals higher intensities than the low resolution ($T21$, lower panels). Besides the intensification in the higher resolution, a weak displacement is observed.

The standard deviations of the dynamical variables (not shown) are of the order of $\sigma_\zeta \sim 10^{-5}$ s^{-1} (vorticity), $\sigma_T \sim 2$ K (temperature), $\sigma_D \sim 10^{-6}$ s^{-1} (divergence), and $\sigma_{p_s} \sim 5$ hPa (surface pressure). Differences (Fig. 2) are shown by the zonally averaged standard deviations of (a) vorticity, (b) temperature, (c) divergence, and (d) surface pressure (high minus low resolution). The differences appear in the regions of maximum standard deviations and are most prominent in the midlatitudes. Note that the difference in the divergence (c) is one order of magnitude smaller than that in vorticity (a). Vorticity and temperature show large differences near the jet streams. The change of the surface pressure variability corresponds to those of vorticity and temperature.

3. Experimental design and methods of analysis

The simulations are performed in the high resolution model with pre-determined parametrizations (1)–(5). In this section the state vector $\mathbf{X}$ comprises the complete set of dynamical variables, vorticity ζ, divergence D, temperature T, and surface pressure p_s. The subscript A describes all wave numbers and L the low wave numbers (large scales) only. Hence $\mathbf{X}_A$ denotes all wave numbers of the variables and $\mathbf{X}_L$ the low wave numbers of the variables (for a schematic overview see Fig. 3). In our study, A corresponds to triangular truncation $T42$ ($\approx 2.5° \times 2.5°$) and the large-scale set L to $T21$ ($\approx 5° \times 5°$).

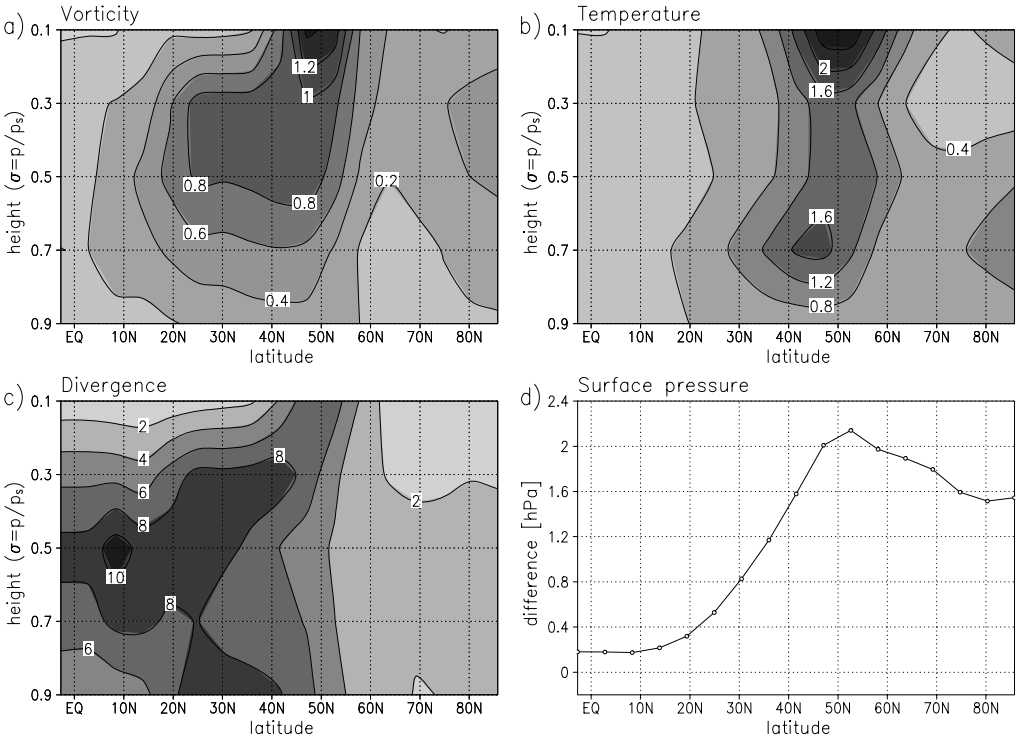

Figure 2. Differences of zonally averaged standard deviations in the high minus a low resolution simulation for (a) vorticity (10^{-5} s^{-1}), (b) temperature (K), (c) divergence (10^{-7} s^{-1}), and (d) surface pressure (hPa).

The dynamic equations can be split into nonlinear (*NLIN*) and linear (*LIN*) contributions. Thus, for the complete set A the equations are written symbolically as

$$\frac{\partial}{\partial t}\mathbf{X}_{\mathrm{A}} = NLIN_{\mathrm{A}}(\mathbf{X}_{\mathrm{A}}) + LIN(\mathbf{X}_{\mathrm{A}}). \tag{7}$$

The subscript A of $NLIN_{\mathrm{A}}$ denotes the nonlinear terms forcing all (A) resolved wave numbers. The dynamics of the low wave numbers is given by the low wave number filter of (7)

$$\left.\frac{\partial}{\partial t}\mathbf{X}_{\mathrm{L}}\right|_{\mathrm{filt}} = NLIN_{\mathrm{L}}(\mathbf{X}_{\mathrm{A}}) + LIN(\mathbf{X}_{\mathrm{L}}) \tag{8}$$

where $NLIN_{\mathrm{L}}(\mathbf{X}_{\mathrm{A}})$ denotes the low wave number filtered couplings between all scales.

The pure large-scale model comprises only low wave numbers $\mathbf{X}_{\mathrm{L}}$ and follows the dynamics

$$\left.\frac{\partial}{\partial t}\mathbf{X}_{\mathrm{L}}\right|_{\mathrm{large}} = NLIN_{\mathrm{L}}(\mathbf{X}_{\mathrm{L}}) + LIN(\mathbf{X}_{\mathrm{L}}). \tag{9}$$

Note that we do not consider different linear processes in the large-scale model since we are interested in the nonlinear interactions. Figure 3 shows that in the large-scale regime the hyperdiffusion of the high resolution simulation (H-42) is negligible compared to the large-scale hyperdiffusion (H-21). The differences between the nonlinear forcings of the large scales in high (8) and low resolution (9) are denoted as residuals

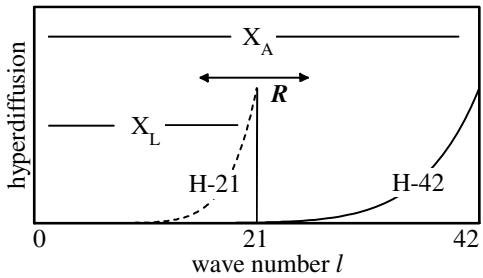

Figure 3. Scale separation for all ($\mathbf{X}_A$) and large-scale variables ($\mathbf{X}_L$) in wave number space. **R** denotes the residual tendencies with upward and downward fluxes across the cut-off scale. The curves show the relative magnitudes of the hyperdiffusion ($\propto \{l(l+1)\}^4$) for high resolution (H-42, solid) and low resolution (H-21, dashed).

(Domaradzki *et al.* 1987)

$$\mathbf{R} = \frac{\partial}{\partial t}\mathbf{X}_L\bigg|_{\text{filt}} - \frac{\partial}{\partial t}\mathbf{X}_L\bigg|_{\text{large}} = NLIN_L(\mathbf{X}_A) - NLIN_L(\mathbf{X}_L). \tag{10}$$

The properties of the residual terms are analysed in the following. In analogy to the state vector **X**, the residual **R** includes R_ζ for the vorticity, R_T temperature, R_D divergence, and R_{p_s} for the surface pressure.

The aim of stochastic parametrization is to mimic the residuals **R** as a stochastic process η in the large scale dynamics

$$\frac{\partial}{\partial t}\mathbf{X}_L\bigg|_{\text{stoch}} = NLIN_L(\mathbf{X}_L) + LIN(\mathbf{X}_L) + \eta. \tag{11}$$

An optimal choice of η should reveal the properties of the high resolution simulation (8).

The residuals **R** are due to the modes, which are unresolved in the low resolution; these are interactions between the high wave numbers and interactions between the high and the low wave numbers. The residuals are large-scale variables and the analysis will show that their dominant intensity is in the highest wave numbers resolved by the low resolution model. Although the residuals look typically wave-like, they do not correspond to meteorological phenomena but represent nonlinear interaction triads with at least one unresolved mode (i.e. wave number higher than $T21$). The residuals include downscale and upscale fluxes. The downscale part is due to the decay of the smallest resolved eddies in the large-scale resolution and can be considered as eddy viscosity. The upscale part describes forcing of resolved modes by unresolved eddies. Due to the unpredictable character of this part, it is possible to consider it as a stochastic process.

To obtain the residuals **R**, a simulation in $T42$ resolution is performed. Additionally, at every time step the large-scale nonlinear tendency terms $NLIN_L(\mathbf{X}_L)$ are used to derive the residuals. There is no parallel simulation required by a purely large-scale model. The experiment is performed on an aqua-planet at equinox with a total duration of 10 years. The $T21$-data are stored every hour corresponding to the integration time step that would be used for PUMA in a low resolution ($T21$) simulation (9).

4. Analysis of subscale forcing

In this section the residuals **R** are analysed. These residuals are large-scale tendencies of the variables, which describe the high wave number mode forcing not included

in a low resolution model. First we present (a) snapshots of the residual fields to obtain qualitative views of their structure, because they serve as the basic dataset of the subsequent analysis. Means and variances of the residuals **R** are determined (b) in grid point and (c) in spectral (wave number) space. The frequency distributions (d) of time series show whether **R** can be considered as a Gaussian process and reveal the role of extreme events. Temporal correlations (e) determine the time-scale of the residuals, and vertical correlations (f) between the model levels indicate whether **R** is vertically coherent. Finally, the correlations of the residuals with the large-scale variables (g) and their hyperdiffusion (h) are determined to unveil whether a part of the subscale forcing can be parametrized using the large-scale variables.

(*a*) *Snapshots*

Some of the characteristic properties of the residuals **R** are visible in the snapshots in Fig. 4. These snapshots show the instantaneous residuals (a) R_ζ for vorticity, (b) R_T temperature, (c) R_D divergence, and (d) R_{p_s} for the surface pressure. The patterns (a)–(c) are derived in the mid-tropospheric model level $\sigma = 0.5$. All patterns are determined at the same time and the residuals are per hour.

The residuals in Fig. 4 share common characteristic properties. The preferred spatial scale in all regions is characterized by the largest wave numbers. Whereas lower absolute values show extended bands, the highest intensity is concentrated in restricted regions. Positive as well as negative residuals are present and both with approximately equal frequency, indicating that the mean vanishes. The major part of the variability occurs in the midlatitudes while in the tropics only weak wave-like patterns are observed. Further inspection shows that these patterns propagate with the mean zonal flow in the midlatitudes.

(*b*) *Spatial distribution*

First the mean value of the residuals is of interest, since non-vanishing deviations imply systematic forcing errors being present in the low resolution model. Since the experiment is zonally symmetric, we consider means of the dynamical variables averaged along latitude circles for the whole simulation time. The zonal means (not shown) are at least one order of magnitude smaller than the standard deviations. The patterns are spatially erratic for vorticity, divergence and surface pressure. The temperature shows a slight deviation from this behaviour with coherent positive residuals in the lower midlatitudes and smaller negative values in the lowest level; all values are below 10% of the standard deviation of the residual. This effect is explained by the different circulation and climate obtained in the higher resolution version of the model. The heating leads to a higher global mean temperature in the higher resolution which amounts to roughly 0.3 K. However, since we cannot exclude that this effect is caused by the model parametrization we cannot attribute this to a general property of the residual forcing. In the following analyses we consider anomalies of the residuals.

In Fig. 5 we show the latitude–height cross-sections of the standard deviations of the residuals of the vorticity, temperature, divergence, and the latitude section for the surface pressure. The standard deviations reveal the following spatial structures:

(a) The vorticity residuals dominate in the mid-tropospheric midlatitudes where they support the eddy-driven jet and are responsible for the enhanced variability of the vorticity (Fig. 2(a)) in the high resolution simulation.

(b) The temperature residuals show largest variability in the lower troposphere of the midlatitudes, with a secondary maximum in the upper polar troposphere.

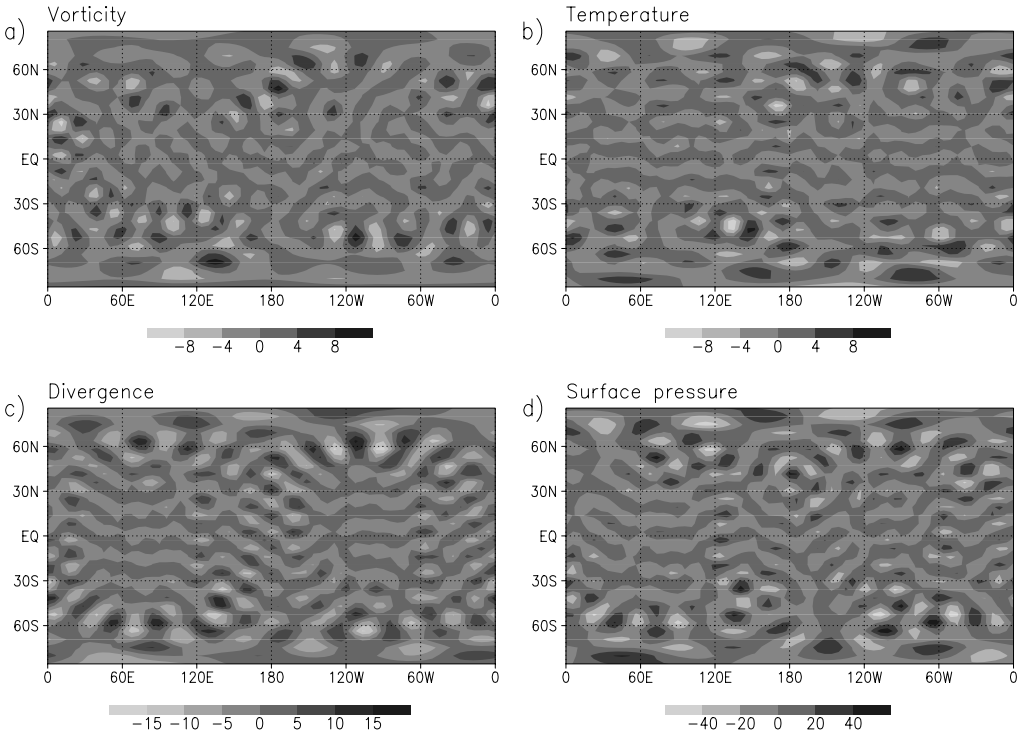

Figure 4. Snapshots of the residuals for (a) vorticity (10^{-7} $s^{-1}h^{-1}$), (b) temperature (10^{-2} K h^{-1}), (c) divergence (10^{-7} $s^{-1}h^{-1}$), and (d) surface pressure (Pa h^{-1}). All terms are forcing per hour (h). Parts (a)–(c) are located in the mid-tropospheric level, $\sigma = 0.5$. Intensities are indicated by the grey scale bars.

(c) The divergence residuals are concentrated in the subpolar troposphere, with a poleward shift compared to the vorticity. The interpretation of this structure is an open problem since it does not correspond to the enhanced variability of the divergence in the tropics (Fig. 2(c)).

(d) The areas with large surface pressure residual correspond to those of the divergence.

The residuals show marked deviations from spatial uniformity. Although the observed spatial distribution hints at unresolved Rossby-wave interactions and surface baroclinicity, an interpretation has to consider that the residuals are differences of nonlinear interaction terms which cannot be directly related to distinct physical processes.

(*c*) *Spectral distribution*

The residual snapshots in Fig. 4 indicate the large contribution of high wave numbers to the residuals. Figure 6 shows the standard deviations of the residuals in the total wave number l and the zonal wave number m domain. For each dynamical variable the level of maximum variance is chosen (see Fig. 5). Vorticity and divergence (a) and (c) are determined in the mid-troposphere ($\sigma = 0.5$) and temperature (b) in the lower troposphere ($\sigma = 0.9$).

The residuals show the largest standard deviations near the highest total wave number $l = 21$. All residuals grow almost linearly with the total wave number and the growth rates are of comparable magnitude. The dependence on the zonal wave number

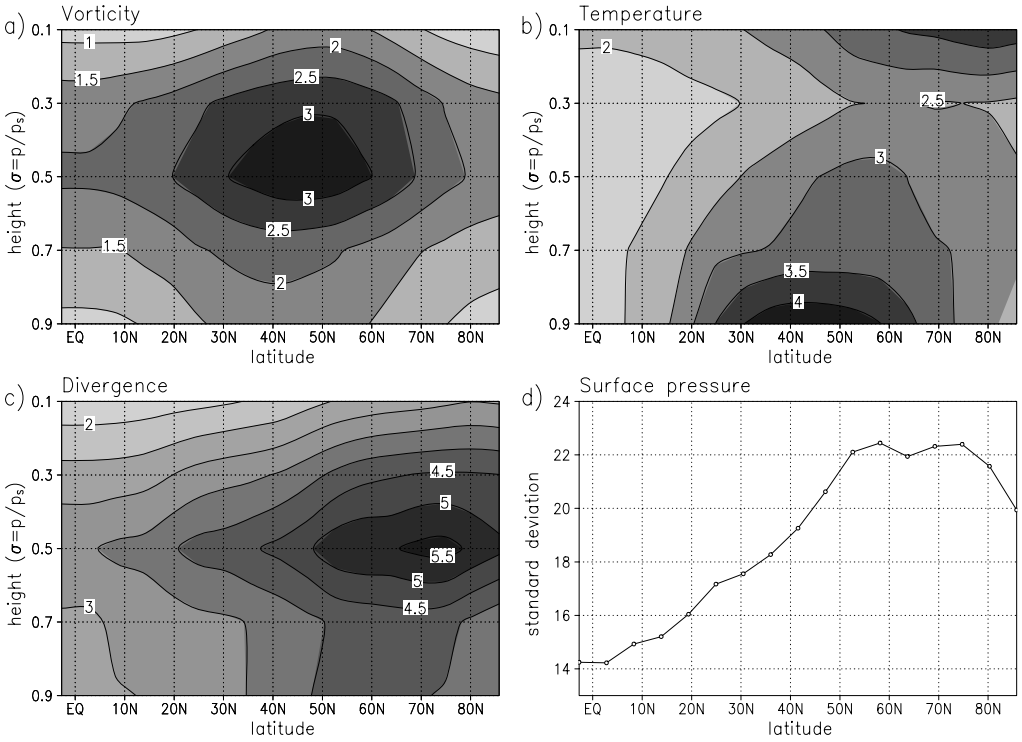

Figure 5. Standard deviations of the residuals for (a) vorticity (10^{-7} s^{-1} h^{-1}), (b) temperature (10^{-2} K h^{-1}), (c) divergence (10^{-7} $s^{-1}h^{-1}$), and (d) surface pressure (Pa h^{-1}). The patterns (a)–(c) show latitude–height cross-sections of the zonal means with isoline intervals 0.5; all terms are forcing per hour (h).

is weak (this confirms turbulence closure theories, see Frederiksen and Davies (1997)). The main result is that the spectra are not white in wave number space.

(*d*) *Frequency distribution*

In addition to the standard deviation, the frequency distribution (FD) of the residuals, and, in particular, the probability of extreme values is relevant for stochastic parametrization. Therefore, for each of the residuals, a time series is analysed representing a grid point of maximum intensity (based on Fig. 5). The FDs are shown in Fig. 7 for (a) vorticity (47°N, $\sigma = 0.5$), (b) temperature (47°N, $\sigma = 0.9$), (c) divergence (70°N, $\sigma = 0.5$), and (d) surface pressure (70°N), on the same longitude.

To detect whether the residuals could be considered as Gaussian variables, a Gaussian distribution is fitted in $R = 0$. The log-plots of the FDs show that for small values of R, a Gaussian distribution is a reasonable fit ($\propto -R^2$ in the log-plot) for all residuals. However, for high values (compared to the standard deviation), the vorticity and temperature residuals cannot be interpreted as Gaussian random variables. Instead, the approximate linear decay of the FDs hints at an asymmetric exponential distribution ($\propto \exp(-|R|)$) with an abrupt decay for negative values. The conclusion derived from this analysis is that in a first approach the forcing is adequately represented by Gaussian noise.

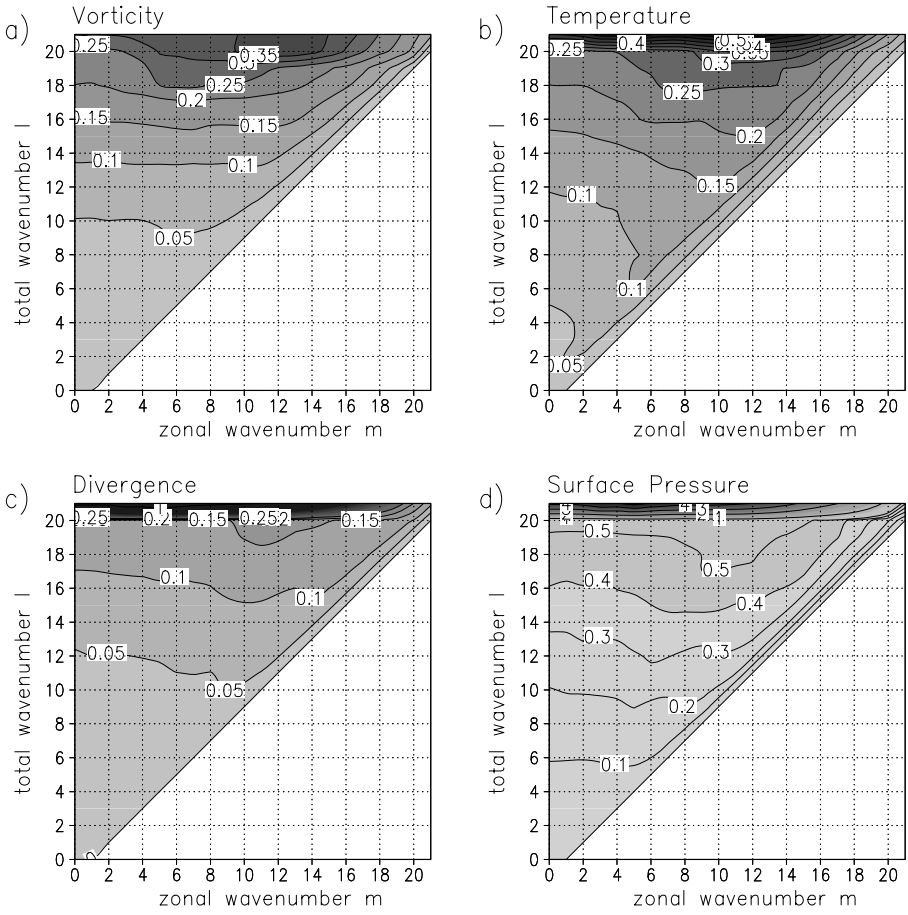

Figure 6. Standard deviation of the residuals vs. total and zonal wave numbers l, m for (a) vorticity (10^{-7} s^{-1}h^{-1}), (b) temperature (10^{-2} K h^{-1}), (c) divergence (10^{-7} s^{-1}h^{-1}), and (d) surface pressure (Pa h^{-1}) (all forcing terms per hour). (a) and (c) are in the mid-troposphere ($\sigma = 0.5$) and (b) in the lowest model level $\sigma = 0.9$. Isoline intervals are 0.05 in (a)–(c) and 0.1 in (d); in (c) and (d), intervals are 1 for isolines ≥ 1.

(*e*) *Temporal correlations*

The temporal behaviour is characterized by the autocorrelation $\langle R(t)R(t+\tau)\rangle/\langle R^2\rangle$ for time lag τ. At individual grid points and levels, two temporal regimes appear:

(i) For small time lags τ (up to about 6 h) the correlation decays algebraically ($\approx 1-\tau^2$) and remains at a high level (>0.9).
(ii) For larger time lags (above about 12 h) the correlation decays exponentially ($\approx \exp(-\tau/T)$) with typical decay times T of the order of one day.

The overall behaviour of the correlations is presented by autocorrelation coefficients for each of the dynamical variables at the time-lag 24 hours. Figure 8 shows the zonal mean of the autocorrelation coefficient for the forcing of the vorticity (a), temperature (b), divergence (c), and surface pressure (d). The maps reveal one day as a characteristic decorrelation time for most of the model levels and latitudes. The correlation is low in the mid-troposphere of the midlatitudes (a)–(c). This can be explained

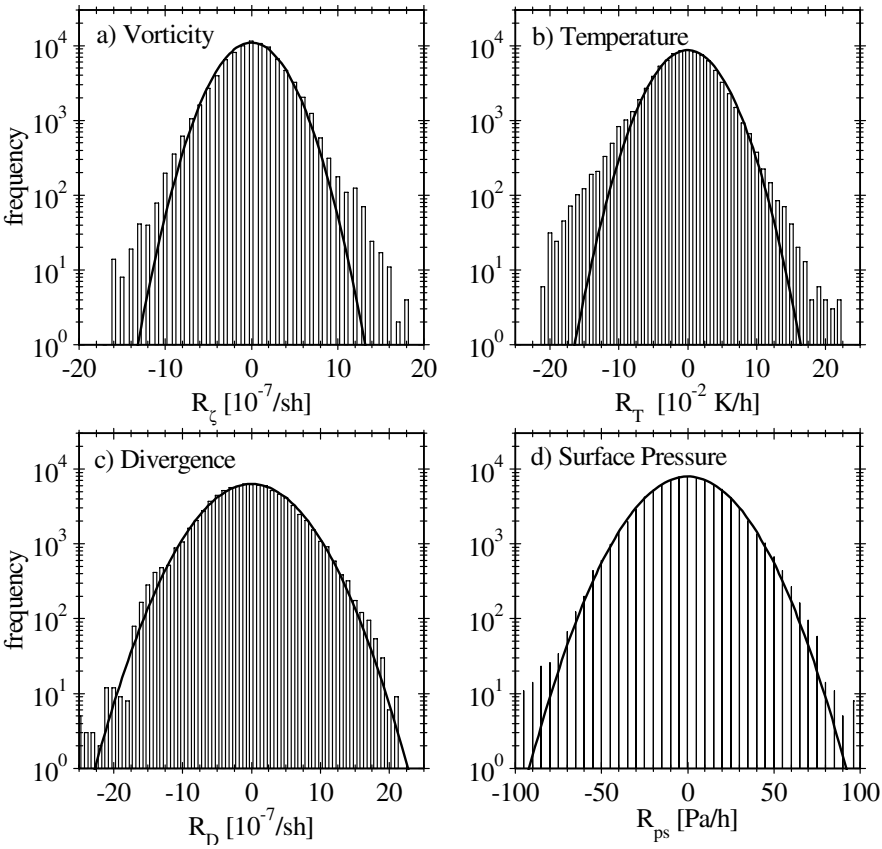

Figure 7. Frequency distribution of residual time series: (a) vorticity (47°N, $\sigma = 0.5$), (b) temperature (47°N, $\sigma = 0.9$), (c) divergence (70°N, $\sigma = 0.5$), and (d) surface pressure (70°N). Solid lines are Gaussian fits centred on $R = 0$.

by the zonal transport (see section 3(a)), which yields a rapid decorrelation at single grid points. All correlations increase towards the poles due to the lower circumpolar advection.

(*f*) *Vertical correlations*

The vertical coherence of the residuals is relevant for interpretation and for modelling as a stochastic process. Therefore, the vertical correlation coefficients between the residuals are determined for vertically adjacent grid points and displayed as zonal means in the intermediate levels $\sigma = 0.2$, 0.4, 0.6, 0.8 (Fig. 9). The correlations differ distinctly for the vorticity (a), temperature (b), and divergence (c): vorticity residuals are mainly correlated between the levels $\sigma = 0.3$ and 0.5 in the midlatitudes. Temperature residuals show an opposite pattern with lowest correlations in the subtropics. In contrast, the divergence residuals are uniformly correlated with the maximum between the model levels $\sigma = 0.3$, 0.5, and 0.7. For a stochastic parametrization the main result is that the dominant part of the forcing shows no vertical coherence.

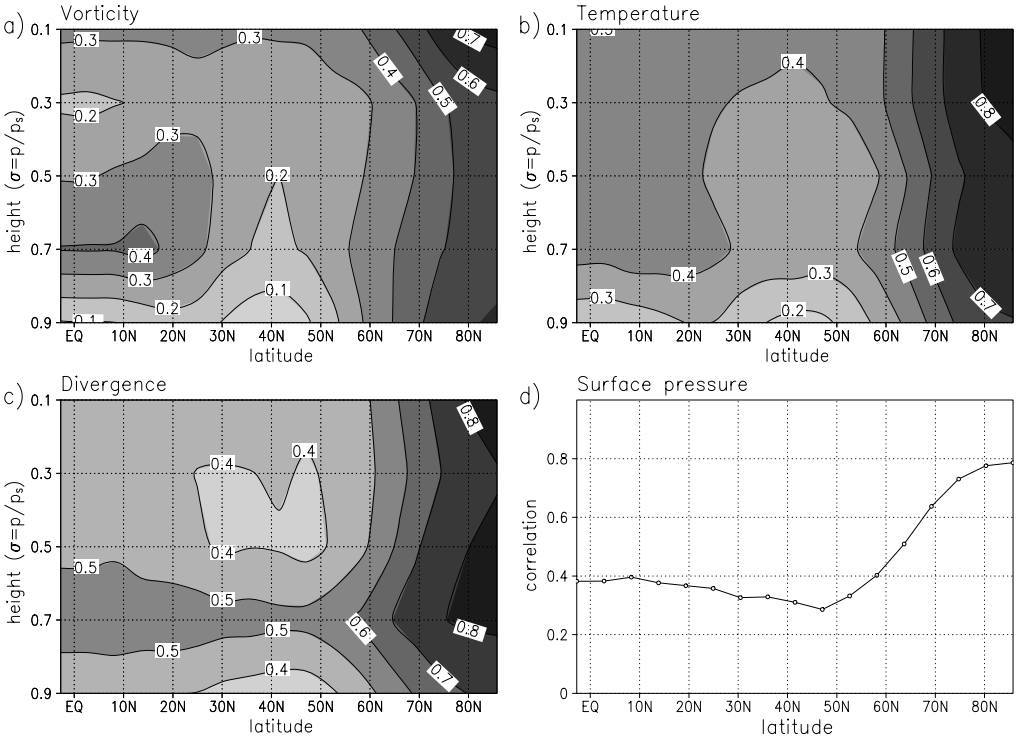

Figure 8. Autocorrelation coefficients of the residual for the lag time $\tau = 24$ h: latitude–height cross-sections for (a) vorticity, (b) temperature, (c) divergence, and (d) surface pressure (vs. latitude), with isoline intervals 0.1 (a)–(c).

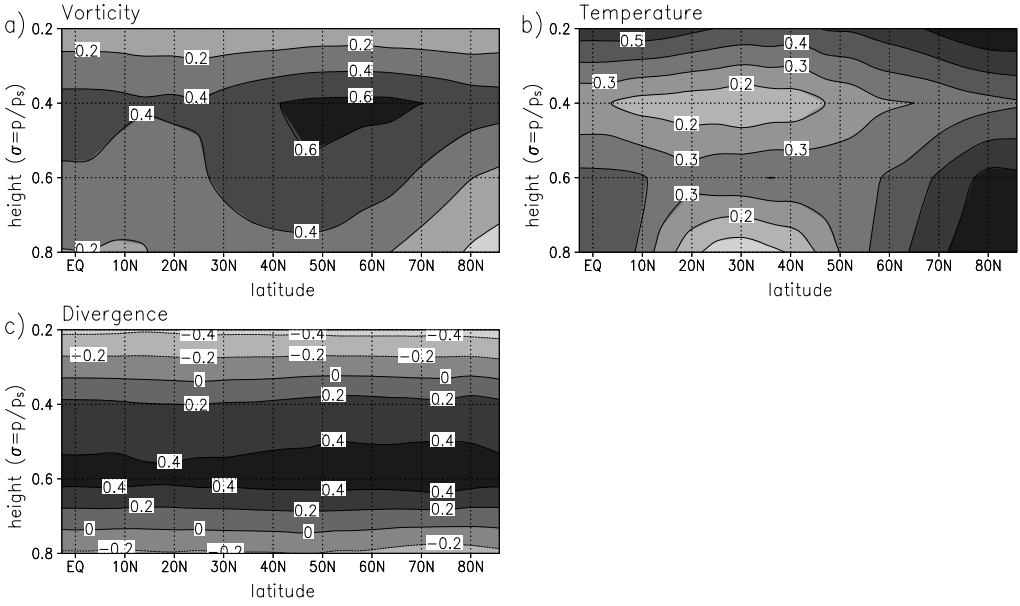

Figure 9. Correlation coefficients of the residuals between the model levels: latitude–height cross-sections of the zonal means for (a) vorticity, (b) temperature, and (c) divergence in $\sigma = 0.2$, 0.4, 0.6, 0.8. Isoline intervals are 0.2 (a) and (c), 0.1 (b).

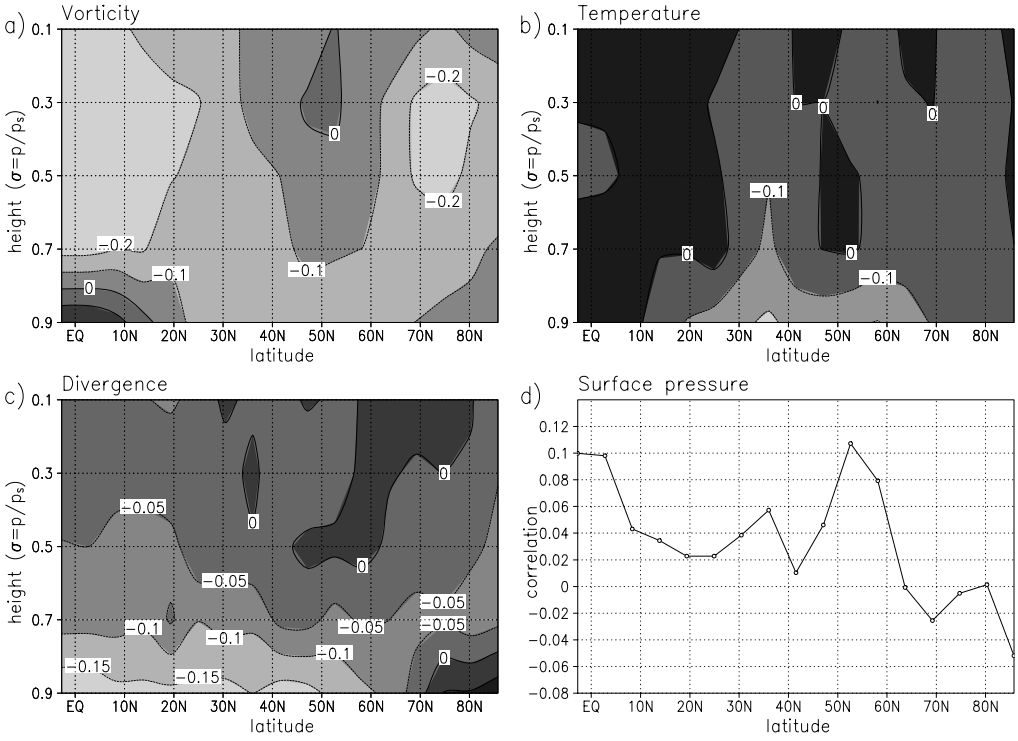

Figure 10. Correlation of the residuals with the corresponding variables for (a) vorticity, (b) temperature, (c) divergence, and (d) surface pressure. Isoline intervals are 0.1 (a) and (b) and 0.05 (c).

(*g*) *Correlation with the variables*

The cross-correlations of the residuals with the large-scale variables may provide guidance for stochastic parametrization in terms of linear processes. Figure 10 shows the correlations between the residuals and the corresponding large-scale variables at each latitude and height for (a) vorticity, (b) temperature, (c) divergence, and (d) surface pressure. The correlations are weakly negative ($-0.2 \ldots 0$) with small positive values for the temperature in the tropics ($0 \ldots 0.1$).

These cross-correlations can be used to estimate a damping time scale τ_X for the variable X:

$$R_X \approx -\frac{1}{\tau_X} X. \tag{12}$$

Based on the cross-correlations c, an estimation for τ_X can be derived by

$$\tau_X \approx -\frac{1}{c}\frac{\sigma_X}{\sigma_{R_X}}. \tag{13}$$

The magnitudes of the standard deviations σ_X of the model variables (not shown) are $\sigma_\zeta \sim 10^{-5}$ s^{-1} for vorticity, $\sigma_T \sim 2$ K for temperature, and $\sigma_D \sim 10^{-6}$ s^{-1} for divergence. The σ_{R_X} values are the standard deviations of the residuals R_X (Fig. 5).

For the vorticity, where the correlation is of the order of -0.1, with $\sigma_{R_\zeta} \sim 2 \times 10^{-7}$ s^{-1}h^{-1}, we can estimate $\tau_\zeta \sim 20$ days. For the temperature, this analysis leads to

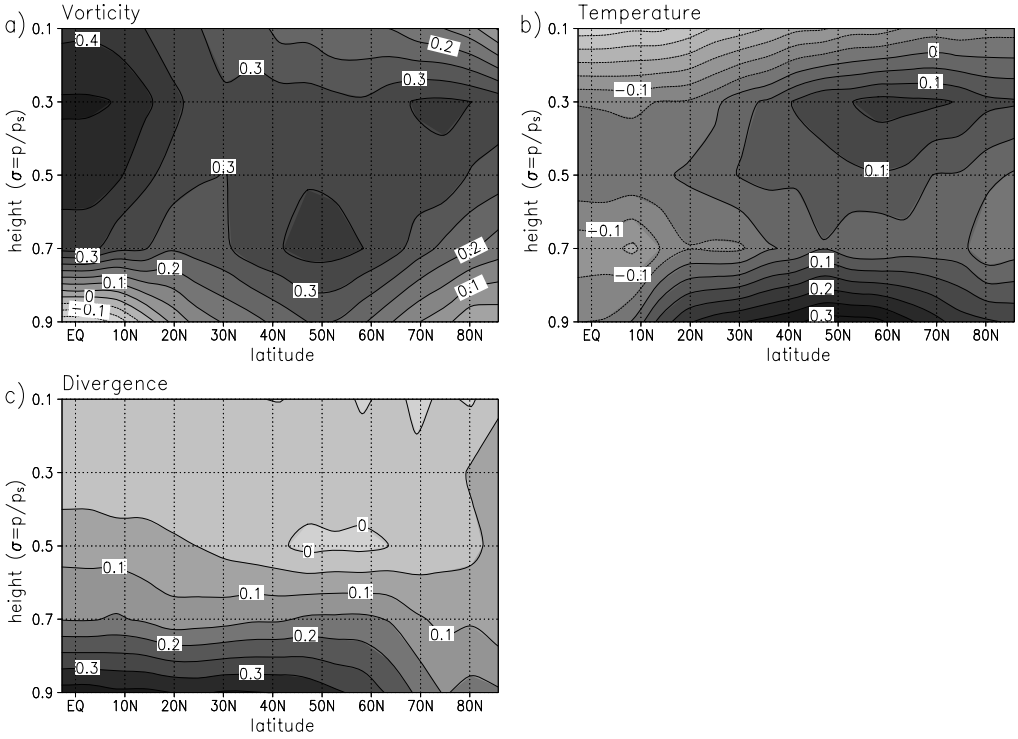

Figure 11. Correlation coefficients of the residuals with hyperdiffusion for (a) vorticity, (b) temperature, and (c) divergence. Isoline intervals are 0.05.

$\tau_T \sim 40$ days with $\sigma_{R_T} \sim 2 \times 10^{-2}$ K h^{-1} and the correlation $c \sim -0.1$. The damping time-scale for the divergence is $\tau_D \sim 2$ days based on $\sigma_{R_D} \sim 4 \times 10^{-7}$ s^{-1}h^{-1} and $c \sim -0.05$. Note that due to the variability of the correlation coefficient, a more exact adjustment is not possible.

(*h*) *Correlation with hyperdiffusion*

The residuals represent two fluxes in the wave number range: an upscale flux to the large scales, which forces the resolved scales, and a downscale flux to smaller scales, which extracts energy from the resolved variables. This downscale flux is conveniently parametrized as a diffusion process with an eddy viscosity. In the PUMA model, this flux is included as hyperdiffusion (6) in the equations for vorticity, temperature and divergence.

To determine the part of the residuals which can be modelled in terms of hyperdiffusion, we correlate the residual with the hyperdiffusion of the corresponding large-scale variable. For example, for the vorticity (1) with hyperdiffusion $H_\zeta = -(-1)^h K \nabla^{2h} \zeta$ we determine $\langle R_\zeta H_\zeta \rangle / (\langle R_\zeta^2 \rangle \langle H_\zeta^2 \rangle)^{1/2}$ at each grid point and level. Figure 11 shows the latitude–height zonal-mean cross-sections of this correlation coefficient for (a) vorticity, (b) temperature, and (c) divergence; note that the surface pressure is not subject to hyperdiffusion.

The residuals of the vorticity (Fig. 11(a)) are positively correlated with the hyperdiffusion in the largest part of the troposphere, with maximum values around 0.4.

The correlations for temperature (b) and divergence (c) are substantial only in the lowest model level. In all variables (a)–(c) negative correlations appear, which are traditionally denoted as 'negative viscosity' (Starr 1968) and describe the accumulation of energy in large scales. Note, however, that in a strict sense, this is reserved for Laplacian diffusion proportional to ∇^2. Here, the small values indicate that this effect is negligible. A main outcome is that the contribution of the dynamic subgrid forcing to hyperdiffusion varies considerably in the troposphere. Note, however, that any modification of the hyperdiffusion has to respect the numerical requirement for smooth fields and that small correlations cannot cause the neglect of hyperdiffusion.

5. Summary and discussion

The forcing of a large-scale model embedded in a high resolution atmospheric model is analysed with the atmospheric circulation model PUMA (Portable University Model of the Atmosphere) based on the primitive equations with Newtonian cooling and Rayleigh friction. The model is run in $T42$ resolution and the embedded model has a lower $T21$ resolution (large-scale model). The subscale forcing due to higher resolution effects is determined as residual tendencies of the nonlinear terms. The main properties are as follows:

1. The residuals have zero mean except for a small temperature forcing which explains the higher global mean temperature in the high resolution model.
2. The variability of the residuals is concentrated in the high total wave number range.
3. The vorticity and divergence residuals are concentrated in the mid-troposphere whereas temperature is mainly forced in the lowest model level.
4. The probability distribution of the residuals is predominantly Gaussian, but shows exponential tails for vorticity and temperature.
5. The decorrelation time is of the order of one day; below 6 hours the residuals remain approximately constant.
6. The correlation between vertical levels is largest for the vorticity and the divergence in the mid-troposphere, but weak for the temperature.
7. The correlations between the residuals and the variables are slightly negative and hint at damping time-scales of 20 days for vorticity, 40 days for temperature and 2 days for divergence.
8. A minor part of the residuals can be considered as hyperdiffusion (correlation up to 0.4); for vorticity in the whole troposphere, for temperature and divergence only in the lowest level.

These results subsume the main statistical properties of the residual tendencies to be used in stochastic parametrizations. A first hint is the concise structure of the residuals: they are dominant in the high total wave number space and, in the vertical, at different heights for each model variable, vorticity, temperature and divergence. Vertical correlations show weak values for vorticity and divergence, whereas the temperature forcing is uncorrelated. The temporal behaviour can be reproduced by an autoregressive process of first order with the decay time of one day. A possible extension of the present study pertains to the downscale energy flux and hyperdiffusion. Although the correlation of the residuals with hyperdiffusion is low (below 0.4), this parametrization, which is common in many atmospheric models, could be improved using the present results (see also Kaas *et al.* (1999)).

In a preliminary test we apply a simplified version of stochastic forcing in the $T21$ resolution of PUMA. The spatial patterns are determined by the spectral intensities

(Fig. 6) derived in section 4(c) with coefficients represented by Gaussian random variables. The random variables are constant up to 6 hours and uncorrelated (white) above, see section 4(e). The effects on the mean circulation and the variability of the model (Figs. 1 and 2) are relatively small. A main reason is that the stochastic forcing (Fig. 6) is located in the spectral range where hyperdiffusion is high (see Fig. 3), which, however, cannot be reduced without loss of stability. Future applications of stochastic parametrization in fully physically parametrized climate models (Fraedrich *et al.* 2005b, 2005c) appear to be more promising, in particular, the prediction of precipitation may benefit. A further useful application of the present approach is that localized forcing terms required in simple linear models of the global atmosphere can be quantified (Zhang and Held 1999).

Acknowledgements

Collaboration with Edilbert Kirk and Frank Lunkeit is appreciated. Discussions while participating (KF) in the ECMWF Workshop on 'Representation of sub-grid processes using stochastic-dynamic models' (June 2005) are gratefully acknowledged. Financial support was given by the Deutsche Forschungsgemeinschaft (SFB-512 and FR450/6).

References

Bartello, P., Métais, O. and Lesieur, M. 1996 Geostrophic versus wave eddy viscosities in atmospheric models. *J. Atmos. Sci.*, **53,** 564–571

Boer, G. J. and Shepherd, T. G. 1983 Large-scale two-dimensional turbulence in the atmosphere. *J. Atmos. Sci.*, **40,** 164–184

Buizza, R., Miller, M. and Palmer, T. N. 1999 Stochastic representation of model uncertainties in the ECMWF Ensemble Prediction System. *Q. J. R. Meteorol. Soc.*, **125,** 2887–2908

Buizza, R., Barkmeijer, J., Palmer, T. N. and Richardson, D. S. 2000 Current status and future developments of the ECMWF Ensemble Prediction System. *Meteorol. Appl.*, **7,** 163–175

Domaradzki, J. A., Metcalfe, R. W., Rogallo, R. S. and Riley, J. J. 1987 Analysis of subgrid-scale eddy viscosity with use of results from direct numerical simulations. *Phys. Rev. Lett.*, **58,** 547–550

Fraedrich, K., Kirk, E., Luksch, U. and Lunkeit, F. 2005a The Portable University Model of the Atmosphere (PUMA): Storm track dynamics and low-frequency variability. *Meteorol. Zeitschrift*, **14,** 735–745

Fraedrich, K., Jansen, H., Kirk, E., Luksch, U. and Lunkeit, F. 2005b The Planet Simulator: Towards a user friendly model. *Meteorol. Zeitschrift*, **14,** 299–304, http://www.mi.uni-hamburg.de/plasim

Fraedrich, K., Jansen, H., Kirk, E. and Lunkeit, F. 2005c The Planet Simulator: Green planet and desert world. *Meteorol. Zeitschrift*, **14,** 305–314

Frederiksen, J. S. and Davies, A. G. 1997 Eddy viscosity and stochastic backscatter parameterizations on the sphere for atmospheric circulation models. *J. Atmos. Sci.*, **54,** 2475–2492

Hoskins, B. J. and Simmons, A. J. 1975 A multi-layer spectral model and the semi-implicit method. *Q. J. R. Meteorol. Soc.*, **101,** 637–655

Hoskins, B., Palmer, T. and Shutts, G. 2004 Stochastic physics. European Centre for Medium-Range Weather Forecasts, http://www.ecmwf.int/about/special_projects/hoskins_stochastic_physica/report_2005.pdf

James, I. N. and Gray, L. J. 1986 Concerning the effect of surface drag on the circulation of a baroclinic planetary atmosphere. *Q. J. R. Meteorol. Soc.*, **112,** 1231–1250

Kaas, E., Guldberg, A., May, W. and Déqué, M. 1999 Using tendency errors to tune the parameterization of unresolved dynamical scale interactions in atmospheric general circulation models. *Tellus*, **51A,** 612–629

Koshyk, J. N. and Boer, G. J. 1995 Parameterization of dynamical subgrid-scale processes in a spectral GCM. *J. Atmos. Sci.*, **52,** 965–976

Kraichnan, R. H. 1976 Eddy viscosity in two and three dimensions. *J. Atmos. Sci.*, **33,** 1521–1536

Lesieur, M. and Rogallo, R. 1989 Large-eddy simulation of passive scalar diffusion in isotropic turbulence. *Phys. Fluids A*, **1,** 718–722

Lin, J. W.-B. and Neelin, J. D. 2000 Influence of a stochastic moist convective parameterization on tropical climate variability. *Geophys. Res. Lett.*, **27,** 3691–3694

2002 Considerations for stochastic convective parameterization. *J. Atmos. Sci.*, **59,** 959–975

Palmer, T. N. 2001 A nonlinear dynamical perspective on model error: A proposal for non-local stochastic-dynamic parametrization in weather and climate prediction models. *Q. J. R. Meteorol. Soc.*, **127,** 279–304

Pérez-Muñuzuri, V., Lorenzo, M. N., Montero, P., Fraedrich, K., Kirk, E. and Lunkeit, F. 2003 Response of a global atmospheric circulation model to spatio-temporal stochastic forcing: Ensemble statistics. *Nonlinear Processes in Geophys.*, **10,** 453–461

Pérez-Muñuzuri, V., Deza, R., Fraedrich, K., Kunz, T. and Lunkeit, F. 2005 Coherence resonance in an atmospheric global circulation model. *Phys. Rev. E*, **71,** 065602(1-4)

Shutts, G. 2001 'Some interpretations of stochastic physical parametrizations.' Pp. 111–126 in ECMWF Proceedings: Key issues in the parametrization of subgrid physical processes 3–7 September 2001, European Centre for Medium-Range Weather Forecasts

Starr, V. P. 1968 *Physics of negative viscosity phenomena.* McGraw-Hill, New York

von Storch, J.-S. 2004 On statistical dissipation in GCM-climate. *Clim. Dyn.*, **23,** 1–15

Theis, S., Hense, A., Damrath, U. and Renner, V. 2003 'Deriving probabilistic precipitation forecasts from LM simulations'. *COSMO Newsletter*, **3,** 209–220

Tran, C. V. and Shepherd, T. G. 2002 Constraints on the spectral distribution of energy and enstrophy dissipation in forced two-dimensional turbulence. *Physica D*, **165,** 199–212

Zhang, Y. and Held, I. M. 1999 A linear stochastic model of a GCM's midlatitude storm tracks. *J. Atmos. Sci.*, **56,** 3416–3435